A Multiscale Approach for Modeling Bubbles Rising in Non-Newtonian Fluids

ARTICLE *in* INDUSTRIAL & ENGINEERING CHEMISTRY RESEARCH · JULY 2011

Impact Factor: 2.59 · DOI: 10.1021/ie2006577

I&EC research
Industrial & Engineering Chemistry Research

ARTICLE

pubs.acs.org/IECR

A Multiscale Approach for Modeling Bubbles Rising in Non-Newtonian Fluids

Xavier Frank,[†] Jean-Claude Charpentier,[†] Youguang Ma,[‡] Noël Midoux,[†] and Huai Z. Li[†,*]

[†]Laboratory of Reactions and Process Engineering, Nancy-University, CNRS 1 rue Grandville, BP 20451, 54001 Nancy Cedex, France

[‡]School of Chemical Engineering and Technology, State Key Laboratory of Chemical Engineering, Tianjin University, Tianjin 300072, P. R. China

ABSTRACT: The present work reports a multiscale approach to describe the dynamics of a chain of bubbles rising in non-Newtonian fluids. By means of the particle image velocimetry (PIV) and the lattice Boltzmann (LB) simulation, a deep understanding of the complex flow pattern around a single bubble is gained at microscale. The interactions and coalescences between bubbles rising in non-Newtonian fluids are experimentally investigated by the PIV measurements, birefringence, and rheological characterization for both an isolated bubble and a chain of bubbles formed from a submerged orifice. Two aspects are identified as central to interactions and coalescence: the stress creation by the passage of bubbles and their relaxation due to the fluid's memory. This competition between the creation and relaxation of stresses displays nonlinear complex dynamics. Along with the detailed knowledge around a single bubble, these fundamental mechanisms governing the bubbles' collective behavior in a train of bubbles at mesoscale leads to cognitive modeling on the basis of behavioral rules. By simulating bubbles as adaptive agents with the surrounding fluid via averaged residual stresses, model predictions for consecutive coalescence between a great number of bubbles compare very satisfactorily with the experimental investigation at macroscale.

1. INTRODUCTION

The bubble behaviors in non-Newtonian fluids play a key role in such diverse fields as decompression sickness, volcanic eruptions, glass manufacture, materials, metallurgy, and various chemical processes. In chemical engineering, typical examples of applications include wastewater treatment, handling and processing of fermentation broths, polymer devolatilisation, bubble column, mechanical stirrer with multiphase, enhanced oil and gas recovery, composites processing, plastic foam processing, etc. Naturally, the rates of heat and mass transfer processes and chemical or biological reactions are essentially governed by the collective behavior of numerous bubbles issued from a multihole distributor: flow field around a bubble, interactions and coalescence between bubbles, bubble size distribution in a column, etc. Also, there is a strong motivation from a theoretical standpoint toward developing a better understanding of the detailed influence of the fluid's rheology on the bubble flow patterns.

In comparison to the state-of-the-art of bubbles in Newtonian fluids,[1] much less is known about the bubble behaviors in non-Newtonian fluids.[2,3] Because of the inherent complex nature of bubble phenomena, a complete theoretical analysis is still impossible at present. An adequate understanding of the bubble hydrodynamics in such media is a prerequisite to studying other transport phenomena like heat and mass transfer with or without chemical reactions. Bubble behaviors can be subdivided into distinct processes: bubble formation from submerged orifices, interaction, and coalescence during the ascent. A somewhat simplified starting point has been the study of bubbles formed from a single submerged orifice. The first major work was reported by Astarita and Apuzzo[4] on the motion of single bubbles. The investigation in this field has been followed by numerous authors, for example, refs 5−9. The results available in the literature provid essentially experimental information on the rise velocity of a single bubble or on the global hydrodynamics and mixing in a bubble column. In particular, a more detailed review on the effects of the fluid's viscoelasticity on bubble shape and velocity can be found in the recent book of Chhabra.[5] Very few investigations on the interactions as well as coalescence between bubbles in such media have so far been reported in the literature.[10,11]

A common feature of the aforementioned phenomena is the existence of a wide range of spatial and temporal scales at which different physical mechanisms happen. Furthermore, these mechanisms of different scales usually interact each other in a nonlinear way to lead to a huge variety of phenomena that underlines the complexity of the subject. Thus, as for the so proposed "the molecular Processes−product−process Engineering (3PE) approach"[12] to describe multidisciplinary nonlinear and nonequilibrium phenomena occurring on different length and time scales in chemical engineering (Figure 1), the bubble behaviors in non-Newtonian fluids could be dealt with an integrated system approach of multiscale modeling. The main idea is to understand how physical, chemical, and interfacial phenomena at a fine scale relate to properties and behavior at a coarser scale, e.g., organizing levels of complexity.[13,14]

In this paper, we highlight a philosophical approach to model bubble behaviors in non-Newtonian fluids at different spatial and temporal scales: detailed information around a single bubble at

Special Issue: Nigam Issue

Received: April 1, 2011
Accepted: July 12, 2011
Revised: July 8, 2011
Published: July 12, 2011

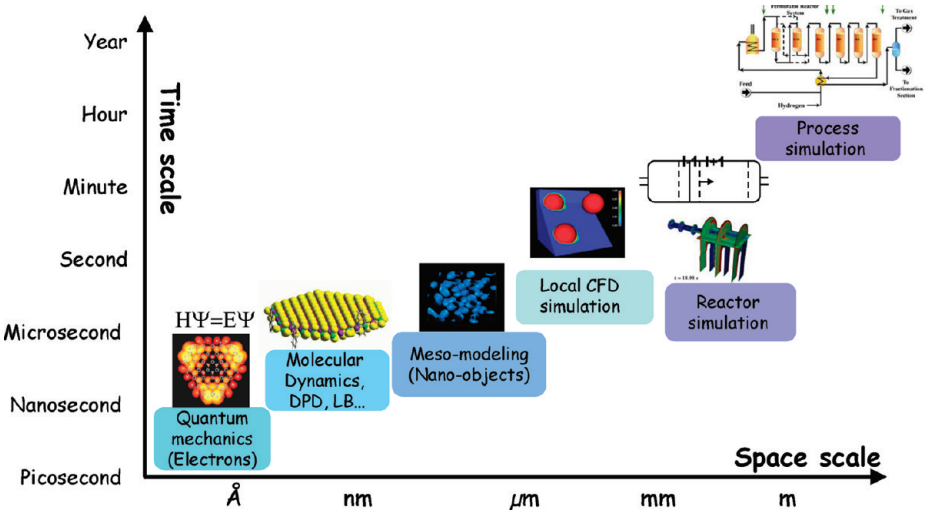

Figure 1. Illustrative view of a modern multiscale spatiotemporal approach in chemical engineering.

microscale by both the fine experiments and numerical simulation; at mesoscale, interactions, and coalescence laws issued from the detailed knowledge around a single bubble; and some illustrative prediction results of macroscopic properties such as the bubble size distribution and comparison with the relative experiments at macroscale. According to the logical order, this paper begins with the study of flow fields around a single bubble followed by the in-line interactions and coalescence between bubbles whose results are essential to global properties in such complex media.

2. EXPERIMENTAL SECTION

In the present study, the experimental setup consists mainly of Plexiglas cylindrical tanks surrounded by a square duct. The role of the square duct is to eliminate optical distortions for visualization as well as to control the liquid temperature inside the cylindrical tank. The diameters of the tanks ranges from 0.20 to 0.30 m, and their height varies from 0.30 to 1.50 m. Air and nitrogen bubble generation is through an orifice of varying diameters ($1-5 \times 10^{-3}$ m) submerged in the liquid in the center of the bottom section of the tanks. An electronic valve of rapid response controlled by a computer permits injection of bubbles of determined volume with the desired injection period T (spatial distance between bubbles). Otherwise, it is possible to inject bubbles under a continuous gas flow rate without the possibility to control the injection period between bubbles. The bubble rise velocity and the frequency of formation or passage are measured by laser probes at different heights. All experiments were carried out at constant temperature. The non-Newtonian fluids used in this work are different concentrations of polyacrylamide (PAAm) and of carboxymethylcellulose (CMC) in water or in water/glycerol mixtures. A rheometrics fluid spectrometer RFS II and an AR 2000 rheometer (TA Instruments) are employed to measure the rheological properties. These fluids behave as shear-thinning fluids and can be fitted for the whole range of the shear rates tested ($\dot{\gamma}$ = 0.01 to 1000 s^{-1}) by the Carreau model

$$\frac{\eta - \eta_\infty}{\eta_0 - \eta_\infty} = [1 + (\lambda\dot{\gamma})^2]^{(n-1)/2} \quad (1)$$

For example, 0.50% PAAm has the following data: η_0 = 38 Pa s, η_∞ = 0.005 Pa s, λ = 45.6 s, and n = 0.29.

Table 1. Rheological Characterization of the 6th Order Maxwell Model for 0.50% PAAm Solution

k	1	2	3	4	5	6
λ_k (s)	0.1	0.5	1	5	10	50
G_k (Pa)	2.81	0.72	1.51	0.66	0.47	0.37

Stress relaxation measurements show that at the same shear rate, the relaxation time ranges from 1 s for diluted CMC solutions to 30 s for concentrated PAAm solutions. Therefore, PAAm solutions may be considered as much more elastic than CMC solutions. To describe the viscoelastic properties of this fluid, a sixth order Maxwell model is developed on the base of rheological measurements

$$G(t) = \sum_{k=1}^{6} G_k \exp\left(-\frac{t}{\lambda_k}\right) \quad (2)$$

A typical example of the measured rheological values is given in Table 1 for the representative fluid of 0.50% PAAm.

Instantaneous velocity fields around a bubble are measured by means of a particle image velocimetry technique (PIV, Dantec Dynamics, Denmark) (Figure 2). Illumination sheets are generated with two pulsed Nd:YAG LASERS (SOLO-I-15 PIV New Wave Research, USA) arranged side-by-side and cross the vertical symmetry axis of the dispersed phase. The energy produced by this source is 2 mJ × 15 mJ. These lasers emit green light with a wavelength of 532 nm for a duration of 8−10 ns. The time between the flashes varies from less than one microsecond to a few milliseconds. The Nd:YAG lasers are also designed to ensure a sequence of illuminations at a frequency of 15 Hz. The laser beams first cross a cylindrical lens, which gave a laser sheet of strong light intensity and small thickness (2 mm maximum). They are focused and superimposed on one zone of measurement. The fluids are inseminated with fluorescent polymer beads (rhodamine B) of 50 μm as seeding particles. An orange filter placed in front of the camera eliminates the reflections of the lasers on the bubbles and lets only the fluorescent light of the particles pass. The size is determined to minimize both Brownian movement and seeding particle sedimentation. The camera, placed perpendicular to the laser sheets, takes two successive

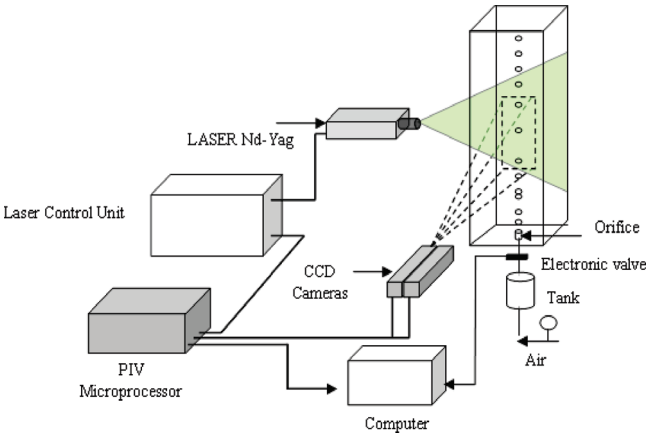

Figure 2. Experimental setup with the PIV and lightning devices.

images at the maximum intensity of the laser pulse. These images are divided into a few thousand small interrogation areas of 16 pixels × 16 pixels. A cross correlation is then performed between the corresponding interrogation areas. When the flow is correctly inseminated, the measurement errors on the velocities are less than 5%. The visualization is carried out by two high-speed digital cameras (VNR 950, Sysma Industrie, France; CamRecord600, Optronis GMBH, Germany) at a rate ranging from 100 to 5000 fps. The light is provided by a halogen light of 800 W, which enlightens the columns via indirect lighting on a white screen behind the bubble column.

3. MULTISCALE APPROACH AND RESULTS

3.1. Flow around a Single Bubble: A Microscopic Description. Direct simulation of flow around a bubble remains a challenging problem for computational fluid dynamics (CFD). The need to explicitly model the dynamics of the interface between different phases and the associated problems of adjusting the computational grid used to compute the flow within each phase present tremendous challenges for conventional fluid simulation approaches. The lattice Boltzmann method is a powerful technique for the computational modeling of a wide variety of complex fluid flow problems.[15] It is a discrete computational method based upon the Boltzmann equation. It considers a typical volume element of fluid to be composed of a collection of particles that are represented by a particle velocity distribution function for each fluid component at each grid point. The time is counted in discrete time steps, and the fluid particles can collide with each other as they move. The rules governing the collisions are designed such that the time-average motion of the particles is consistent with the Navier−Stokes equation.

Within the lattice Boltzmann (LB) framework, the fluid is described at the molecular level in a statistical way. Molecules are forced to move on a lattice that is a discretization of the phase space. We used here the so-called D2Q9 lattice, a bidimensional lattice, on which particles' velocity can have only nine values, including zero. Evolution of the system with the discrete time t consists in a streaming stage, where molecules move from their node and reach a neighboring node, and a collision stage, where molecules collide and velocities are consecutively modified. Molecules are not implemented directly but described in a statistical way by means of the particle probability distribution functions (PPDF)f_i, where $f_i(\vec{r},t)$ is the number of molecules having the velocity $\vec{c}_i$ at the point $\vec{r}$ and time t. Useful quantities are deduced from PPDF and molecules' velocities

$$\rho = \sum_i f_i \tag{3}$$

$$\rho\,\vec{u} = \sum_i f_i\,\vec{c}_i \tag{4}$$

The time evolution of PPDF obeys the LBGK (Lattice Bhatnagar−Gross−Krook) equation that is nothing but a simplification of the general lattice Boltzmann equation

$$f_i(\vec{r} + \delta t\,\vec{c}_i, t + \delta t) - f_i(\vec{r}, t) = -\frac{1}{\tau_r}(f_i - f_i^{eq}) + \frac{\vec{a}(\vec{c}_i - \vec{u})}{{c_s}^2} f_i^{eq}\delta t \tag{5}$$

Distributions f_i^{eq} are equilibrium polynomial expression and computed with the following conserved quantities

$$\sum_i f_i^{eq} = \rho$$

$$\sum_i f_i^{eq}\,\vec{c}_i = \rho\,\vec{u} \tag{6}$$

$$\sum_i f_i^{eq} c_{i\alpha} c_{i\beta} = \rho u_\alpha u_\beta + P_{\alpha,\beta} - \Gamma_{\alpha,\beta}$$

where $P_{\alpha,\beta}$ is the pressure tensor deduced from a free energy scheme[16−18] and $\Gamma_{\alpha,\beta}$ the viscoelastic stress tensor.

It is worth noting that the viscoelastic stress tensor $\Gamma_{\alpha,\beta}$ is computed with the help of a modified sixth order Maxwell model

$$\Gamma_{\alpha,\beta} = \sum_{k=1}^{6} \Gamma_{\alpha,\beta}^k$$

$$\frac{\partial \Gamma_{\alpha,\beta}^k}{\partial t} = G_k D_{\alpha,\beta} - \frac{1}{\lambda_k'}\Gamma_{\alpha,\beta}^k \tag{7}$$

$$D_{\alpha,\beta} = \partial_\alpha u_\beta + \partial_\beta u_\alpha$$

In order to take the shear thinning into account, λ_k' is modified relaxation time stemming from λ_k

$$\lambda_k' = \frac{\eta(\phi)}{\sum_{k'=1}^{6} \lambda_{k'} G_{k'}} \tag{8}$$

where the viscosity $\eta(\phi)$ is deduced from the Carreau model with the help of a phenomenological quantity $\phi(\vec{r},t)$ to describe its temporary evolution

$$\frac{\eta(\phi) - \eta_\infty}{\eta_0 - \eta_\infty} = [1 + (\lambda\phi)^2]^{(n-1)/2}$$

$$\frac{\partial \phi}{\partial t} = -\frac{\phi - \sqrt{|I_D{}^{(2)}|}}{t_r} \tag{9}$$

$$t_r = \frac{t_{r0}}{1 + \frac{\phi}{\phi_0}}$$

dx.doi.org/10.1021/ie2006577 |Ind. Eng. Chem. Res. 2012, 51, 2084–2093

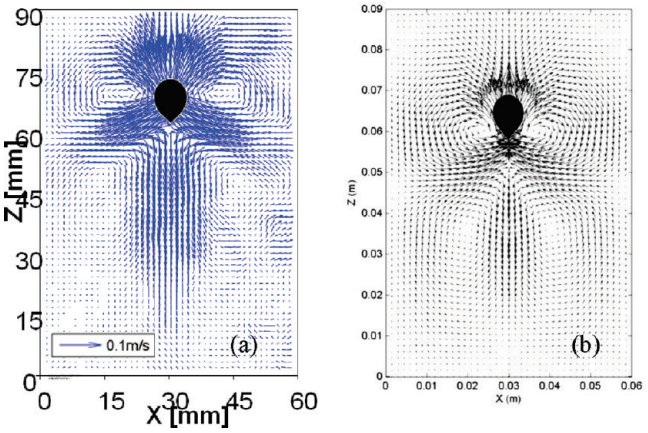

Figure 3. Flow field around a rising bubble of 190 × 10^{-9} m^3 in 1% (wt) PAAm solution: (a) experimental measurements by the PIV device and (b) LB simulation with computed bubble shape.

where $I_D^{(2)}$ is the second invariant of the tensor $D_{\alpha,\beta}$, and the reference values used in the present simulation are respectively t_{r0} = 12s, ϕ_0 = 0.5 s^{-1}.

This rheological approach was dynamically validated through successive relaxation experiments.[17,18]

To perform bubbly flow simulations at microscale, a gas−liquid model is required. The free energy-based model seems suitable to simulate bubbles in both Newtonian and non-Newtonian fluids.[16,17] To describe both hydrodynamics and multiphase patterns in binary fluids, two densities, ρ_A and ρ_B, are necessary with a total density $\rho = \rho_A + \rho_B$ and a density difference $\Delta\rho = \rho_A - \rho_B$. As ρ and $\vec{u}$ are implemented through PPDF f_i as in single phase flows, the density difference $\Delta\rho$ is computed from g_i, another PPDF function obeying a LBGK equation too

$$g_i(\vec{r} + \delta t\,\vec{c}_i, t + \delta t) - g_i(\vec{r}, t) = -\frac{1}{\tau_r}(g_i - g_i^{eq}) \quad (10)$$

Equilibrium distribution functions g_i^{eq} are then deduced to conserve the following quantities

$$\sum_i g_i^{qe} = \Delta\rho$$

$$\sum_i g_i^{eq}\,\vec{c}_i = \Delta\rho\,\vec{u} \quad (11)$$

$$\sum_i g_i^{eq} c_{i\alpha} c_{i\beta} = \Delta\rho u_\alpha u_\beta + \Delta\mu\delta_{\alpha,\beta}$$

The chemical potential difference $\Delta\mu$ is deduced from a free energy scheme.[16−18] The non-Newtonian properties, including viscoelastic ones, of the fluids were implemented in the LB scheme on the basis of a modified sixth order Maxwell fluid coupled to shear-thinning effects.

The flow fields around an individual bubble in these solutions have very peculiar features. The flow in front of the bubble is very similar to that in the Newtonian case. In the central wake, the movement of the fluid is surprisingly downward. Finally, a hollow cone of upward flow surrounds this negative wake. This conical upward flow zone begins on the sides of the bubble and is largely extended backward (Figure 3). The real typical shape of the bubble is also added in Figure 3 to locate the position of the bubble. Obviously, the bubble's shape in the non-Newtonian fluids differs much from that in Newtonian case. Small bubbles

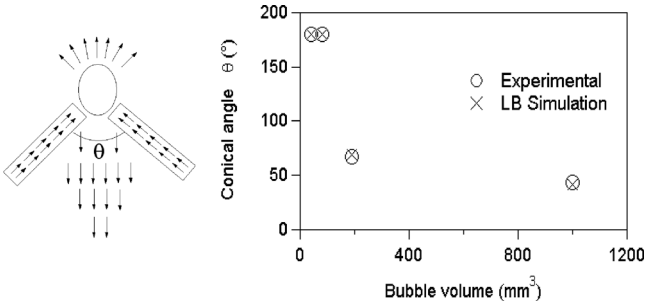

Figure 4. Schematic representation of the flow field around a bubble rising in viscoelastic fluids and variation of the conical angle with the bubble volume in 0.50% (wt) PAAm: experiments vs LB simulation.

are elongated vertically and have a teardrop shape. With a further increase in volume, bubbles take the flattened shape, however, with always a tail behind the bubble. In the past, the negative wake was initially investigated by both qualitative visualization[19] and the use of LDA[3,20] at a point in a non-Newtonian fluid; however, our results show clearly the global shape of the negative wake, in particular the conical upward flow zone around the negative wake. It is worth noting that the conical open angle θ decreases with the bubble's volume and tends to an asymptotic value in these fluids (Figure 4). These detailed flow patterns were extensively investigated by the PIV device in our group in function of the fluids' viscoelesticity.[21,22] The spatial distribution of stresses around a bubble between the conical ascension and the central negative wake was also quantified by the birefringence method. The fluid's viscoelasticity was identified as responsible for the origin of the negative wake.[23]

Figures 3 and 4 show the main features computed by the LB approach around a single bubble. The theoretical flow field exhibits effectively the negative wake, a conical positive flow around the negative wake with an open angle too. The comparison with the experimental measurements is quite satisfactory, including the bubble shape. The main advantage of the LB approach with respect to a direct numerical scheme is the possibility to explore very elastic fluids through the above-mentioned viscoelastic tensor. Moreover, the shape evolution of the bubble could also be computed as a direct consequence within the framework of a two-component and binary LB scheme.

Clearly, both the high resolution of about 50 μm of the PIV device and the microscopic equations used in the LB approach provide a solid foundation for understanding the various physical phenomena at microscale around a single bubble in non-Newtonian fluids.

3.2. In-Line Interactions and Coalescence between Bubbles: Mesoscopic Modeling. *3.2.1. In-Line Interactions between Bubbles: A Linear Competing Mechanism of Stresses.* With the help of the electronic valve controlled by the PC, it is possible to modulate the injection period T between two consecutive bubbles instead of the continuous injection of a gas flow rate. The evidence for in-line interactions between bubbles is clearly brought up in this work: the rise velocity decreases with the increase in the injection period T for a given bubble volume (Figure 5). A sufficiently long injection period is necessary to prevent the interactions between bubbles. When the injection period became short enough (<1 s), coalescence occurs. In particular, a significant factor differentiating bubble−bubble interactions in non-Newtonian fluids from that in water is the long field of action. So, we have the idea to simulate the passage of bubbles by imposing

consecutive shear rates (pulses) to a fluid sample by means of the rheometer RFS II that measures the response of the sample in terms of shear stress. We call this original approach rheological simulation[24] that is performed in these fluids in the cone-and-plate geometry of the rheometer, taking especially into account the experimental values of rise velocity and injection period. There is a gradual accumulation of residual stresses tending asymptotically toward a stationary value. The magnitude of these residual stresses could be considered as both strongly dependent upon the injection period and proportional to the elasticity of the fluid.

To provide new evidence of the residual stresses after the passage of bubbles in non-Newtonian fluids, birefringence measurements are also carried out with a chain of bubbles rising in these fluids. In panel (a) of Figure 6, a typical example of the spatial stress distribution around two bubbles in 1% PAAm is presented. White zones illustrate the existence of axisymmetric stresses, in front of the bubble due to the fluid compression and especially behind the bubble because of the residual stresses, while black zones owing to the extinction of the polarized light characterize the absence or small magnitude of stress. It is clear that the trailing bubble can enter in the large field of residual stresses behind the leading one and provoke either interactions through pure acceleration of rise velocity or coalescence for closer intervals between bubbles. This illustrates visually the mechanism of in-line bubble interactions and coalescence.

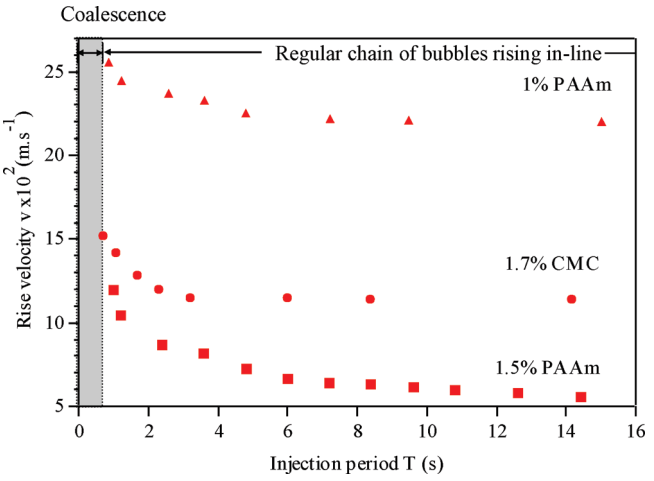

Figure 5. Linear in-line interactions between bubbles: decrease of the rise velocity with the injection period before reaching an asymptote after a characteristic period depending upon the fluid and bubble volume. Orifice diameter $d_0 = 2 \times 10^{-3}$ m, bubble volume $V_B = 1.37 \times 10^{-6}$ m^3.

Even if the flow field exhibits a negative wake behind a leading bubble as shown in panel (b) of Figure 6 by the PIV or panel (c) of Figure 6 by the LB simulation, the rise velocity increases for the whole train of bubbles as well. This flow configuration is totally different from that in Newtonian fluids. The wake hypothesis cannot explain the acceleration of bubbles because it tends to suggest that bubbles will decelerate. These results suggest clearly that another mechanism should be discovered for interactions in non-Newtonian fluids. In light of above findings, the following scenario can be proposed: after the passage of a leading bubble, the memory effect of the fluid holds the shear-thinning process during a certain time so that the local viscosity decreases and induces the acceleration of the rise velocity of the trailing bubble. Unambiguously, the mechanism governing the in-line bubble interactions is a dynamical competition between the creation and relaxation of stresses[25]

$$\frac{d\tau}{dt} + \alpha\tau = \beta\dot{\gamma} \qquad (12)$$

For example, typical values are $\alpha = 1$ s^{-1} and $\beta = 10$ Pa for 0.50% PAAM solution.

This memory effect of the residual stresses of preceding bubbles on the rise velocity of a bubble train is successfully modeled by means of the linear superposition principle to compute the acceleration of the rise velocity of a regular bubble train due to the temporary decrease of a local viscosity (Figure 7).

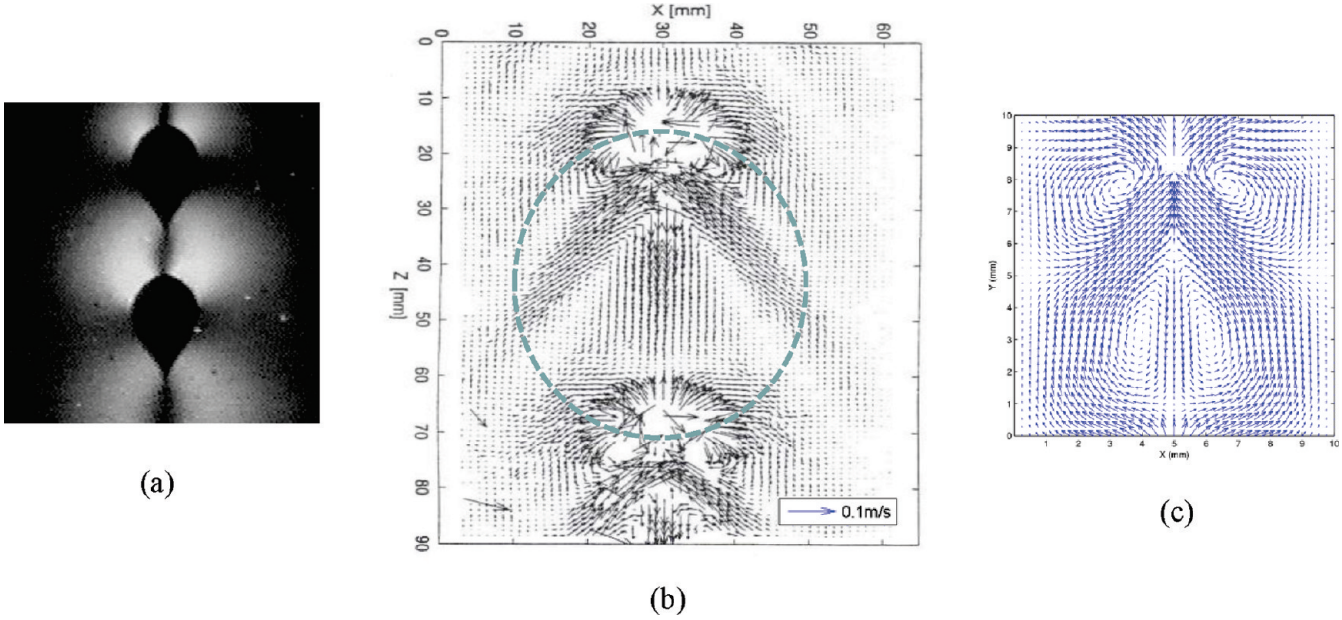

Figure 6. In-line interactions between a train of bubbles rising in 1% (wt) PAAm solutions: (a) birefringence visualization, (b) flow field measured by the PIV, and (c) LB simulation.

3.2.2. Nonlinear and Chaotic Coalescence between Bubbles: Cognitive Modeling. Above a threshold that depends on the nature of each fluid, especially the viscoelasticity, the interactions are no longer linear as the coalescence occurs (Figure 8): a regular bubble chain is broken up. The regularity of the bubble formation at the orifice[26] and the dynamical competition between the creation and relaxation of stresses lead naturally to the theory of chaos. In order to understand the coalescence nature, the time delay embedding method of reconstructing the phase−space diagram was applied to time series data (bubble passage) recorded at different heights in the bubble column. The calculation of several parameters, the largest Lyapunov exponent, the correlation dimension, the power spectrum and the phase portraits, indicates that the coalescence between bubbles is chaotic.[27,28] Experimentally, the chaos' appearance can also be described by the period-doubling sequences. It is worth noting that the variation of the correlation dimension with the embedding dimension shows that the chaos is deterministic with a limited number of degrees of freedom. As shown in Section 3.3, this is also confirmed by the macroscopic evolution of the bubble number at different heights in the column. In fact, the bubble number normalized by the total number of bubbles generated at the orifice for a fixed duration (typically about 3000 bubbles) levels off a plateau before falling due to the consecutive coalescence. The plateau corresponding to the constant bubble number in the inertial rise stage increases inversely with the fluid viscosity. The decrease in the bubble number in the higher column section is bounded by an asymptotic value due to the limited capacity of bubble generation at the orifice. This shows explicitly that the complexity of the in-line bubble coalescence in non-Newtonian fluids cannot degenerate into an arbitrary nature. Intuitively, the collective behaviors of bubbles in such media obey underlying fundamental laws.

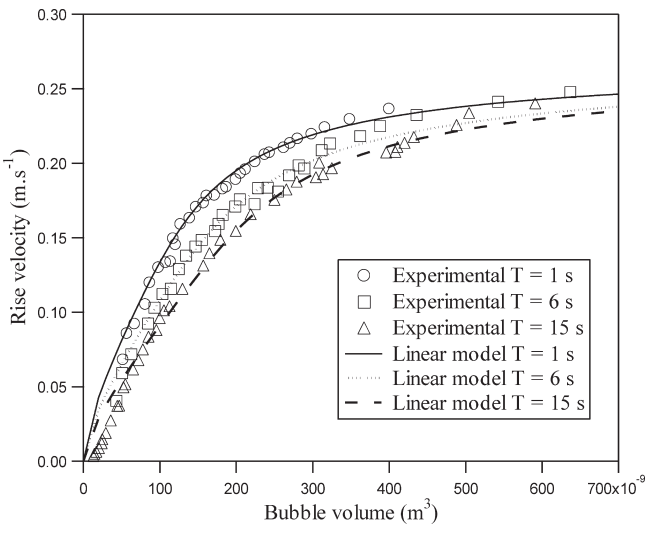

Figure 7. Comparison of the rise velocity of a bubble train between the theoretical linear modeling and experimental data in 0.5% PAAm with three injection periods.

Certainly, the LB simulation could be applied to simulate the complex interactions between bubbles as shown in panel (c) of Figure 6. However, it is worth noting that the LB is very CPU memory and time-consuming for the computation. Recently, some physicists and biologists[29,30] are trying to explore a new way to describe the complex evolving systems such as an anthill, a central nervous system, or ecosystems. Even though these complex systems differ in detail, the question of coherence under change is the central enigma for each. General principles usually rule the behavior of these *complex adaptive systems* (CAS), principles that point to ways of solving the attendant problems. The task of formulating theory for these systems is more than difficult as the collective behavior of such a system is not a simple juxtaposition of the behaviors of its parts. The main quest is to extract these general principles and to shape them into building blocks for a new scientific approach.

If we want to understand the interactions of large numbers of agents, we must be able to describe the capabilities of individual agents. It is quite logic to suppose that an agent's behavior is determined by some elementary rules. Stimulus−response rules are typical and simple: IF stimulus *S* occurs, THEN response *R* is given. In an anthill, the stimuli could be pheromones deposed by other ants in search of food; the response could be the moving direction according to the magnitude of pheromones. The collective behavior of the whole anthill would privilege the shortest way to go to the food source with progressive increase on the pheromones' intensity as each ant passing through this way would drop new pheromones. Therefore, we can establish qualitatively an ethnological analogy between bubbles and ants. They interact both between them through the interactions with their environment: pheromones for ants and residual stresses in fluid for bubbles (Figure 9). To some extent, there is a connection between an ant and a bubble as an individual agent as well as between the concentration of pheromones and the magnitude of stresses. This is experimentally confirmed by the injection of a sheared fluid through a syringe voluntarily displaced from the rise axe of the train of bubbles: because of the reduced viscosity in the sheared fluid, a rising bubble takes a bend to enter in the zone of reduced viscosity. The residual stresses left by this bubble guide the passage of trailing bubbles owing to the minimized drag, and the modified rise axe can be self-maintained as well as

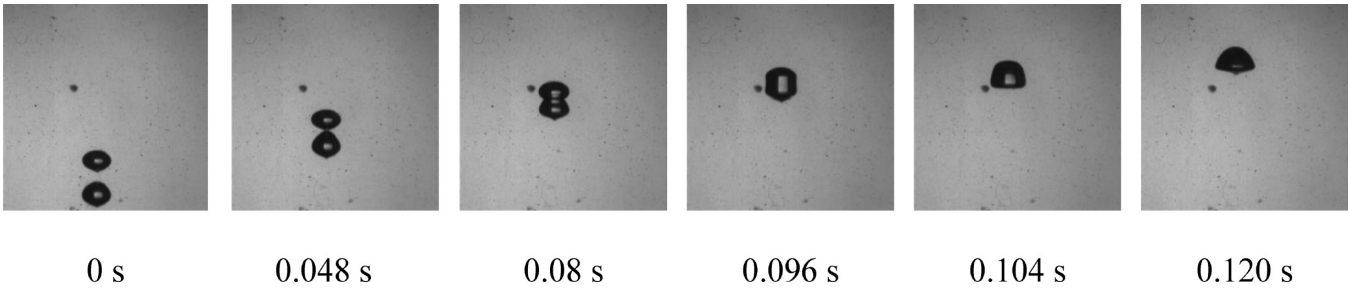

Figure 8. Coalescence between in-line rising bubbles.

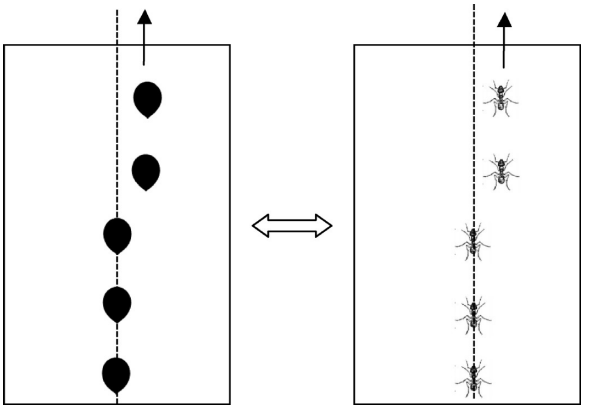

Figure 9. Communication similarity between agents: bubbles rising in non-Newtonian fluids through residual stresses (reduced drag) and an anthill through pheromones.

the displacement is not too large with respect to the initial vertical axe.

Our immediate objective is to find a simple syntax for IF/THEN rules that depend critically on the way an agent (a bubble) interacts with its environment (fluid) and other agents (bubbles). Starting from the knowledge of the interactions and coalescence between bubbles, we adopt the following strategy as the cognitive approach that specifies the bubble's capacities at a fixed point in fluid in time. The three basic elements of this approach are a set of detectors, a set of IF/THEN rules, and a set of effectors. The detectors represent the bubble's capacities for extracting information from its environment (residual stresses in fluid, presence of other bubbles). The IF/THEN rules describes its capacities for processing that information (accelerating or not the rise velocity, coalescence or not). The effectors are its ability to act on the environment (leaving its own residual stresses according to its size).

The total fluid height is divided into 20000 cells in which the stresses are continuously computed according to the passage of consecutive bubbles. Each cellule represents a height of 75 μm and is supposed to display homogeneous stresses whose evolution is estimated by the dynamical competition between the creation (passage of bubbles) and relaxation of stresses (memory effects) of the first order (eq 12).

As a first approximation, the bubble is considered as spherical with an equivalent diameter d_{eq}. With an added mass, the motion equation of a bubble is described by a classical balance of different forces: inertial, buoyancy, and drag

$$\left(\rho_G + \frac{11}{16}\rho_L\right)V_B\frac{dU}{dt} \approx \frac{11}{16}\rho_L V_B\frac{dU}{dt} = F_b - F_t \qquad (13)$$

where the buoyancy force is $F_b = (\rho_L - \rho_G)V_B g$, and the drag force is $F_t = (1/2)AC_D\rho_L U^2$ with $A = (\pi d_{eq}^{\ 2})/4$.

After the passage of a preceding bubble, the memory effect of the fluid holds the shear-thinning process during a certain time so that the local viscosity decreases and induces the acceleration of the rise velocity of the trailing bubble. The estimation of the local effective viscosity is made through a virtually additional shear rate corresponding to the residual stresses

$$\begin{cases} \tau = \eta_m\dot{\gamma}_m \\ \eta_m = \eta_\infty + (\eta_o - \eta_\infty)[1 + (\lambda\dot{\gamma}_m)^2]^{(n-1)/2} \end{cases} \qquad (14)$$

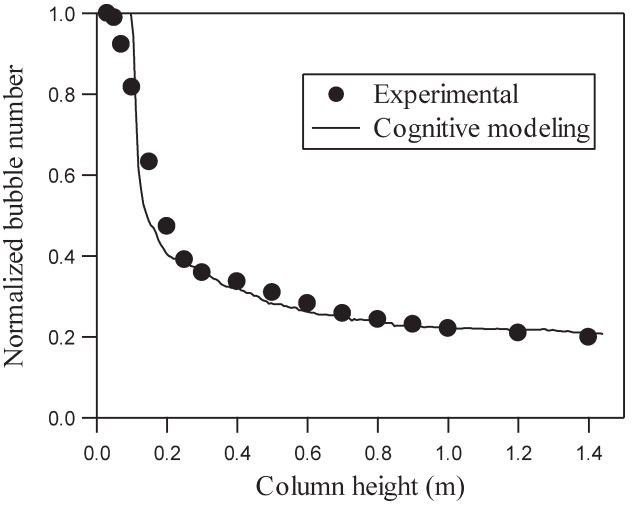

Figure 10. Comparison of the variation of the normalized bubble number with the column height in 0.5% PAAm solution between the experiments and cognitive modeling for 3000 bubbles.

In the present study, we use simply, as a first approximation, the characteristic shear rate

$$\dot{\gamma}_B = U/d_{eq} \qquad (15)$$

It is clear that the sum of these two shear rates leads to an effective viscosity

$$\eta_e = \eta_\infty + (\eta_o - \eta_\infty)\{1 + [\lambda(\dot{\gamma}_B + \dot{\gamma}_m)]^2\}^{(n-1)/2} \qquad (16)$$

For a bubble rising initially at U, the main rules have then the form:

- IF (there are residual stresses in a cellule τ), THEN (compute the new increased velocity U' via η_e).
- IF (two bubbles enter in contact), THEN (coalescence takes place to form a new bigger bubble $V_B = V_{B1} + V_{B2}$ and compute the new rise velocity U').

These rules are based on the physical mechanisms understood at the mesoscopic level and could be hopefully expected to predict the interactions and coalescence between a great number of bubbles to come close to the industrial scale. In particular, the experimental results[27,28] show that the coalescence between bubbles rising in-line takes place easily in non-Newtonian fluids. The film drainage is mainly encountered in Newtonian fluids or for the lateral coalescence between bubbles in non-Newtonian fluids.

It is worth noting that the relaxation is a very complex procedure in polymer solutions. The cognitive approach employed in this study is to make use of averaged value of a temporarily relaxed local viscosity in the wake of a preceding bubble instead of complex and detailed local flow fields. Otherwise, the computation for the interactions and coalescence between a great number of bubbles will be excessively time consuming.

3.3. In-Line Interactions and Coalescence between Bubbles in a Bubble Column: Macroscopic Properties. Instead of dealing with the complexity of interactions and coalescence between a great number of bubbles rising in a bubble column at macroscopic scale, the mesoscopic interactions rules deduced from the understanding of the microscopic mechanisms are then

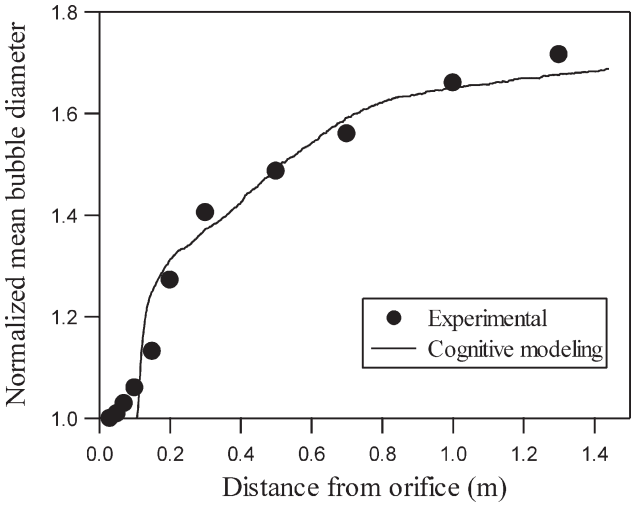

Figure 11. Comparison of the increase in the normalized bubble diameter with the column height in 0.5% PAAm solution between the experiments and cognitive modeling for 3000 bubbles.

applied to follow numerically the ascension of 3000 bubbles consecutively generated at the orifice in a bubble column filled up with a fluid of 1.50 m height. The total fluid height is represented by 20000 individual rectangular cellules as the simulation box. As the inlet condition, identical bubbles are regularly injected through an orifice at the bottom of the column with the experimental values of the period T. For the outlet condition, a bubble reaching the top of the column is eliminated for the following time step. A simple counter allows us to impose periodic bubbling in the numerical simulation. The coalescences takes place when two bubbles get in touch due to the acceleration of the rise velocity of a trailing bubble with the reduced drag. These two bubbles form then a bigger one, according to the mass conservation, and its new rise velocity is computed with the new coalesced size.

The computation is implemented on a classical PC, and several statistical quantities are stored at different heights in the column. Some illustrative results are given as follows in two PAAm solutions. Figure 10 shows a comparison of the local bubble number normalized by 3000 injected at total at different heights between the experiments and the computing from the mesoscopic cognitive approach. The global tendency is well described by this approach even though the local curve details are not perfect. The small difference results essentially in the mean values used of α and β for bubbles of different size instead of more accurate values for each size. With respect to the orifice, a minimum height that depends on the viscoelasticity is required to accumulate sufficient residual stresses to induce the first coalescence. With the increasing sequence of coalescences between bubbles, the number of bubbles decreases significantly with height. In contrary, the bubble size increases because of the consecutive coalescences. Figure 11 represents the evolution of the bubble diameter normalized by the initial one in function of the fluid height. It is interesting to note that both the bubble number and the bubble diameter tend to asymptotic values as stated before; this indicates indirectly a bounded complexity due to mainly a constant injection flow rate of gas at the orifice as a limited resource and then a signature of deterministic chaos. These macroscopic behaviors predicted by the mesoscopic cognitive approach are particularly noteworthy as they emerge naturally without special fitting. In addition, a close analysis reveals that the

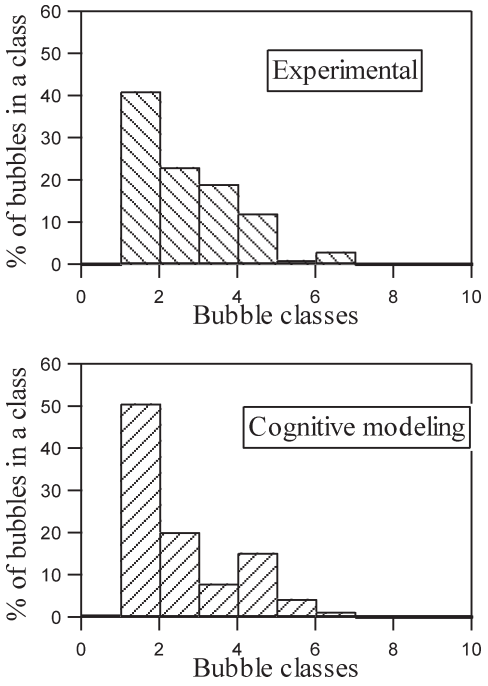

Figure 12. Bubble class distribution at a height of 0.40 m from the orifice in 0.75% PAAm solution, air flow rate $Q = 200 \times 10^{-9}$ m^3 s^{-1}. Comparison between the experimental results and cognitive modeling.

present mesoscopic modeling describes satisfactorily experimental details such as the intermediate distribution of bubble classes at different column heights (Figure 12). These macroscopic data are indispensable for the design, operation, and improvement of an industrial installation through the local knowledge of the bubble size distribution, gas holdup, specific interfacial area, etc. Detailed numerical intermediate values allow also signal treatments, for example, application of wavelets, bifurcation sequence analysis,and route to chaos. Obviously, this new approach captures important quantitative and qualitative features of the collective behaviors of bubbles at the macroscopic level from the knowledge of detailed physical and interfacial phenomena at microscopic and mesoscopic levels.

Certainly, the current approach is still limited to the dynamics of a single rising train of bubbles. In industrial reality, the multihole distributor injects numerous trains of bubbles, rising not only in line but also in parallel. The mutual interactions and eventual coalescences between lateral bubble trains should then be included in the multiscale approach. This is an avenue that we are currently exploring.

4. CONCLUSIONS

In this paper, the concept of a multiscale modeling approach is highlighted with which physical phenomena at different scales can be investigated. We have developed a comprehensive study on the collective behaviors of a chain of bubbles rising in non-Newtonian fluids in view of simulating an industrial bubble column one day. A coherent picture begins to emerge on the basis of fundamental physical understanding at different scales. By means of both the experimental PIV and the lattice Boltzmann simulation based on the particle dynamics, the detailed flow and stress features around a single bubble in different viscoelastic fluids are well understood at the microscale. The proposed LB scheme

interfaced with a viscoelastic model captures successfully the main flow features such as the complex negative wake, its physical origin, the bubble's teardrop shape, and the spatial stress distribution around a bubble rising in a non-Newtonian fluid. These various fine experimental tools such as the PIV device, rheological stimulus−response simulation, and birefringence visualization are also applied to the investigation of a train of bubbles at mesoscale with the main focus on the nature of interactions and coalescences between bubbles. The dynamical competition between the creation of stresses after the passage of bubbles and the relaxation of these stresses forming temporarily a corridor of reduced viscosity is clearly identified as the principal mechanism governing in-line interactions and coalescences. Along with the detailed information gained by both the experiments and theoretical LB simulation, this knowledge of an in-line train of bubbles is resumed as synthetic behavioral laws at mesoscale. An ethnological similitude can be drawn for the communicating agents between them through interactions with their environment: the evolution of the pheromone concentration deposed by ants on a favored passage in an anthill and the residual stresses left by the passed bubbles to guide trailing bubbles through a drag reduction in the fluid. Good agreement of the simulation results with experimental data is achieved for a train of numerous bubbles rising in a column at macroscale for various operating parameters at different heights such as the bubble number, mean bubble diameter, bubble class distribution, etc.

Our results elucidate then the nature of in-line interactions and coalescence between bubbles rising in line in viscoelastic non-Newtonian fluids. However, it is still far from an industrial bubble column where great populations of bubbles rise, interact, and coalesce not only in line but also in parallel. Further studies are then required to include this lateral spatial dimension in the multiscale modeling approach. It is envisaged that the present study could lay the foundation for a better comprehension of bubble dynamics in these complex media.

AUTHOR INFORMATION

Corresponding Author

*E-mail: Huai-Zhi.Li@ensic.inpl-nancy.fr.

ACKNOWLEDGMENT

The financial support provided by the French Ministry of Research, the National Centre for Scientific Research (CNRS), and the Program FSH with industrial companies (GDF, IFP-EN, Schlumberger) is gratefully acknowledged.

NOTATION

C_D = drag coefficient
$\vec{c}_i$ = lattice velocity
D_o = orifice diameter (m)
D_{max} = maximum bubble diameter (m)
DPD = Dissipative Particle Dynamics
F = force (N)
LB = Lattice Boltzmann
P = pressure (Pa)
$P_{\alpha,\beta}$ = pressure tensor
Q = gas flow rate ($m^3\ s^{-1}$)
$\vec{r}$ = lattice location
T = injection period between bubbles (s)
t = time (s)
U,U' = bubble rise velocity ($m\ s^{-1}$)
$\vec{u}$ = fluid velocity ($m\ s^{-1}$)
V_B = bubble volume (m^3)

Greek Letters

α = stress relaxation parameter (s^{-1})
β = stress creation parameter (Pa)
$\Gamma_{\alpha,\beta}$ = viscoelastic stress tensor
$\dot{\gamma}$ = shear rate (s^{-1})
$\Delta\mu$ = chemical potential difference
η = viscosity (Pa s)
κ = adiabatic coefficient
θ = angle between the normal to the bubble surface at any element and the vertical axis
λ = relaxation time in Carreau model (s)
λ_k = kth relaxation time in Maxwell model (s)
ρ_L = fluid density ($kg\ m^{-3}$)
ρ_G = gas density ($kg\ m^{-3}$)
σ = surface tension ($N\ m^{-1}$)
$\boldsymbol{\tau}$ = stress tensor
τ = stress (Pa)
τ_r = relaxation time (s)

REFERENCES

(1) Clift, R.; Grace, J. R. Weber, M. E. *Bubbles, Drops and Particles*; Academic Press: New York, 1978.
(2) Debregeas, G.; de Gennes, P. G.; Brochard-Wyart, F. The life and death of bare viscous bubbles. *Science* **1998**, *279*, 1704–1706.
(3) Hassager, O. Negative wake behind bubbles in non-Newtonian liquids. *Nature* **1979**, *279*, 402–403.
(4) Astarita, G.; Apuzzo, G. Motion of gas bubbles in non-Newtonian liquids. *AIChE J.* **1965**, *11*, 815–820.
(5) Chhabra, R. P. *Bubbles, Drops & Particles in Non-Newtonian Fluids*, 2nd ed.; CPC Press: Boca Raton, 2006.
(6) Rodrigue, D. A simple correlation for gas bubbles rising in power-law fluids. *Can. J. Chem. Eng.* **2002**, *80*, 289–292.
(7) Fan, W. Y.; Ma, Y. G.; Jiang, S. K.; Yang, K.; Li, H. Z. An experimental investigation for bubble rising in non-Newtonian fluids and empirical correlation of drag coefficient. *J. Fluids Eng.* **2010**, *132*, 021305.
(8) Haque, M. W.; Nigam, K. D. P.; Joshi, J. B.; Viswanathan, K. Studies on mixing time in bubble columns with pseudoplastic solutions. *Ind. Eng. Chem. Res.* **1987**, *26*, 82–86.
(9) Haque, M. W.; Nigam, K. D. P.; Joshi, J. B. Hydrodynamics and mixing in highly viscous pseudoplastic non-Newtonian solutions in large diameter bubble columns. *Chem. Eng. Sci.* **1986**, *41*, 2321–2331.
(10) Acharya, A.; Ulbrecht, J. Note on the influence of viscoelasticity on the coalescence rate of bubbles and drops. *AIChE J.* **1978**, *24*, 348–351.
(11) De Kee, D.; Chhabra, R. P.; Dajan, A. Motion and coalescence of gas bubbles in non-Newtonian polymer solutions. *J. Non-Newtonian Fluid Mech.* **1990**, *37*, 1–18.
(12) Charpentier, J. C. Among the trends for a modern chemical engineering, the third paradigm: The time and length multiscale approach as an efficient tool for process intensification and product design and engineering. *Chem. Eng. Res. Des.* **2010**, *88*, 248–254.
(13) Charpentier, J. C. The triplet "molecular processes-product-process" engineering: The future of chemical engineering? *Chem. Eng. Sci.* **2002**, *57*, 4667–4690.
(14) Luo, K. H.; Xia, J.; Monaco, E. Multiscale modelling of multiphase flow with complex interactions. *J. Multiscale Modell.* **2009**, *1*, 125–156.
(15) Succi, S. *The Lattice Boltzmann Equation for Fluid Dynamics and Beyond*; Clarendon Press: Oxford, 2001.

(16) Frank, X.; Funfschilling, D.; Midoux, N.; Li, H. Z. Bubbles in a viscous liquid: Lattice Boltzmann simulation and experimental validation. *J. Fluid Mech.* **2006**, *546*, 113–122.
(17) Frank, X.; Li, H. Z. Complex flow field around a bubble rising in non-Newtonian fluids. *Phys. Rev. E* **2005**, *71*, 036309.
(18) Frank, X.; Li, H. Z. Negative wake behind a sphere rising in viscoelastic fluids: A lattice Boltzmann investigation. *Phys. Rev. E* **2006**, *74*, 056307.
(19) Sigli, D.; Coutanceau, M. Effect of finite boundaries on the slow laminar isothermal flow of a viscoelastic fluid around a spherical obstacle. *J. Non-Newtonian Fluid Mech.* **1977**, *2*, 1–21.
(20) Bisgaard, C. Velocity fields around spheres and bubbles investigated by laser-Doppler anemometry. *J. Non-Newtonian Fluid Mech.* **1983**, *12*, 283–302.
(21) Funfschilling, D.; Li, H. Z. Flow of non-Newtonian fluids around bubbles: PIV measurements and birefringence visualisation. *Chem. Eng. Sci.* **2001**, *56*, 1137–1141.
(22) Frank, X.; Li, H. Z.; Funfschilling, D.; Burdin, F.; Ma, Y. Bubble motion in non-Newtonian fluids and suspensions. *Can. J. Chem. Eng.* **2003**, *81*, 483–490.
(23) Kemiha, M.; Frank, X.; Poncin, S.; Li, H. Z. Origin of the negative wake behind a bubble rising in non-Newtonian fluids. *Chem. Eng. Sci.* **2006**, *61*, 4041–4047.
(24) Li, H. Z.; Frank, X.; Funfschilling, D.; Diard, P. Bubbles' rising dynamics in polymeric solutions. *Phys. Lett. A* **2004**, *325*, 43–50.
(25) Frank, X.; Li, H. Z. An analytical approach to the rise velocity of periodic bubble chains in non-Newtonian fluids. *Europ. Phys. J. E* **2005**, *16*, 29–35.
(26) Li, H. Z.; Mouline, Y.; Midoux, N. Modelling the bubble formation dynamics in non-Newtonian fluids. *Chem. Eng. Sci.* **2002**, *57*, 339–346.
(27) Li, H. Z.; Mouline, Y.; Choplin, L.; Midoux, N. Chaotic bubble coalescence in non-Newtonian fluids. *Int. J. Multiphase Flow* **1997**, *23*, 713–723.
(28) Jiang, S. K.; Ma, Y. G.; Fan, W. Y.; Yang, K.; Li, H. Z. Fractal and chaotic behaviour of bubble coalescence in non-Newtonian fluids: A multiscale analysis. *Korean J. Chem. Eng.* **2011**, *28*, 56–63.
(29) Gell-Mann, M. *The Quark and the Jaguar: Adventures in the Simple and the Complex*; Wiley: Hoboken, NJ, 1994.
(30) Holland, J. H. *Adaptation in Natural and Artificial Systems: An Introductory Analysis with Applications to Biology, Control and Artificial Intelligence*, 2nd ed.; MIT Press: Cambridge, MA, 1992.